Journal Pre-proofs

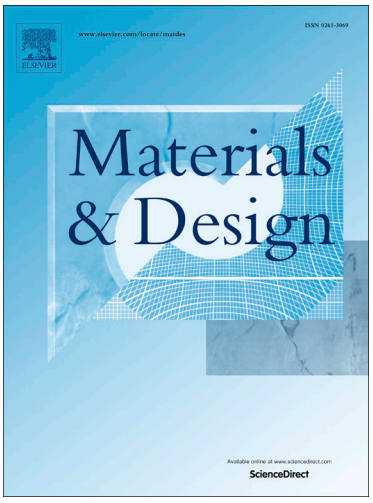

Physico-chemical Modification of Gelatine for the Improvement of 3D Printability of Oxidized Alginate-gelatine Hydrogels Towards Cartilage Tissue Engineering

T. Kreller, T. Distler, S. Heid, S. Gerth, R. Detsch, A.R. Boccaccini

PII: S0264-1275(21)00430-5
DOI: https://doi.org/10.1016/j.matdes.2021.109877
Reference: JMADE 109877

To appear in: *Materials & Design*

Received Date: 18 February 2021
Revised Date: 23 April 2021
Accepted Date: 5 June 2021

Please cite this article as: Kreller, T., Distler, T., Heid, S., Gerth, S., Detsch, R., Boccaccini, A.R., Physico-chemical Modification of Gelatine for the Improvement of 3D Printability of Oxidized Alginate-gelatine Hydrogels Towards Cartilage Tissue Engineering, *Materials & Design* (2021), doi: https://doi.org/10.1016/j.matdes.2021.109877

Physico-chemical Modification of Gelatine for the Improvement of 3D Printability of Oxidized Alginate-gelatine Hydrogels Towards Cartilage Tissue Engineering

T. Kreller[1*], T. Distler[1*], S. Heid[1], S. Gerth[2], R. Detsch[1], A. R. Boccaccini[1§]

[1]Institute of Biomaterials, Department of Materials Science and Engineering, Friedrich Alexander-University Erlangen-Nürnberg, 91058 Erlangen, Germany
[2]Fraunhofer Institute for Integrated Circuits IIS

[*]Equal contribution
[§]Corresponding author: aldo.boccaccini@fau.de

Keywords:
Hydrogels; Oxidized Alginate; Gelatine; 3D Printing; Tissue Engineering

Abstract

This work explored 3D bioplotting to mimic the intrinsic hierarchical structure of natural articular cartilage. Alginate dialdehyde-gelatine (ADA-GEL) was used as a hydrogel ink to create hierarchically ordered scaffolds. In comparison to previously reported ADA-GEL compositions, we introduce a modified formulation featuring increased amounts of thermally modified gelatine. Gelatine was degraded by hydrolysis which resulted in tailorable printability characteristics further substantiated by rheological analysis. ADA(3.75%w/v)-GEL(7.5%w/v) with gelatine modified at 80 °C for 3 h could be printed in hierarchical complex structures reaching scaffold heights of over 1 cm. The hierarchical structure of the scaffolds was confirmed via µ-CT analysis. To examine mechanical properties as well as the suitability of the hydrogel as a proper matrix for cell seeding and encapsulation, nanoindentation was performed. Elastic moduli in the range of ~ 5 kPa were measured. Gelatine heat pre-treatment resulted in modifiable mechanical and rheological characteristics of ADA-GEL. In summary, this study demonstrates the possibility to enhance the printability of ADA-GEL hydrogels to fabricate hierarchical scaffold structures with shape stability and fidelity, without the necessity to change the initial hydrogel chemistry by the use of additives or crosslinkers, providing a valuable approach for fabrication of designed scaffolds for cartilage tissue engineering.

1. Introduction

Osteoarthritis is the most common joint disease of the adult human being. Mostly caused by inherent form- and function disorders, illnesses or accidents almost every 10th adult human in Germany suffers from osteoarthritis [1]. In particular, women and men aged between 50 to 70+ years are affected. Within the course of the disease, the guiding symptoms are severe pain and the loss of function of joint units like knee-, hip- or shoulder joints due to the degeneration of hyaline cartilage tissue. Hyaline cartilage is the highly specialized connective tissue of diarthrodial joints. Its principal function is to provide a smooth, lubricated surface for articulation and to facilitate the transmission of loads with a low frictional coefficient [2]. Up to date osteoarthritis is not curable. Consequently, the goal of osteoarthritis therapy is focused on pain reduction and on long-term preservation of the hyaline cartilage tissue to secure its functionality [3]. If conservative therapies like physiotherapy and medical treatments cannot grant a normal daily routine for the patient, surgery is required. State of the art are autologous osteochondral transplants (AOT) as well as matrix-linked autologous chondrocyte transplants (MACT) to restore cartilage tissue. For both types of surgery cartilage tissue is taken out of a healthy host tissue environment. In the case of AOTs, healthy cartilage-bone fragments are placed upon the damaged area. However, the newly formed tissue by the AOT approach is mainly fibrocartilage, which is not useful for a long-term cure [4,5]. In the case of MACTs, on the other hand, chondrocytes get isolated from the sample, increased in numbers, linked to a matrix and are implanted in damaged cartilage parts. Thanks to this technique, hyaline-like tissue can be formed with similar characteristics as native cartilage tissue [1]. The use of three-dimensional (3D) scaffolds in combination with chondrocytes, however, could rapidly accelerate the healing process thanks to the manifold applications of scaffolds as space-filling agents, as delivery vehicles for bioactive molecules and as three-dimensional structures that organize cells and feature stimuli for an even better-directed formation of the desired tissues [6]. To manufacture 3D scaffolds, biofabrication techniques attract increasing interest worldwide [7]. Especially in the fields of regenerative medicine and tissue engineering, biofabrication has great potential thanks to the numerous opportunities that are offered by additive manufacturing technologies such as 3D-bioplotting. Using such technologies enables scientists to manufacture complex tissue constructs consisting of the plotted material as well as encapsulated cells which leads to better biomimetic approaches to replicate native tissue [8]. However, as biofabrication represents an advanced tissue engineering approach, the current state-of-the-art therapy in the clinic involves still the seeding of cells on pre-fabricated scaffolds. Hence, the development of suitable materials for hierarchical bioprinting to manufacture advanced scaffold matrices for MACT is a current major challenge that must be overcome. For this application, hydrogels are promising materials because they can mimic the microenvironment of natural tissues and therefore can promote cell attachment, growth, and proliferation [9]. In this context, specifically

naturally-derived hydrogels provide important characteristics like biocompatibility and promising cell-material interactions that path the way for developing a native ECM (*extracellular matrix)* analogue structure [6]. Synthetic approaches, in contrast, may often lack integrin-binding ligands which hinder cell attachment and proliferation [10]. Since the ECM is mostly composed of polysaccharides, glycosaminoglycans, and various proteins, ADA-GEL *(alginate dialdehyde–gelatine)* with a polysaccharide as well as the collagen derived component gelatine (Fig. 1) provides a promising matrix for biomimetic tissue engineering applications [11]. The potential of ADA-GEL for bioprinting approaches has been demonstrated [12–14]. However, mechanical demands in physiological conditions remain challenging for hydrogels with thermoresponsive characteristics. Therefore, the mechanical properties of ADA-GEL systems need to be tailored for the specific application. Due to physico-chemical modifications of the structure, crosslinking, and the use of additives it is possible to obtain hydrogels with modifiable viscous, rheological, and mechanical properties [11,15]. Potential additives include micro-and nanofibers as well as micro-and nanoparticles. Nanocellulose in particular is being investigated as a promising additive, as not only mechanical properties could be improved with it, but also cell proliferation, bioadhesion, and viability [16,17]. In a dual-crosslinking approach, we have shown that the mechanical properties [18] and crosslinking of ADA-GEL can be tailored by crosslinking the alginate-based component using $CaCl_2$ and the gelatine component enzymatically with microbial transglutaminase [19]. This work aimed to investigate the possibility of recreating the intrinsic hierarchical structure of articular cartilage found *in-vivo* by a bioplotting approach *in-vitro*. Due to its promising characteristics regarding biocompatibility, biodegradability, and cell-material interactions, ADA-GEL is used as a hydrogel-ink [20]. Hydrogel precursor modification via temperature pre-treatment of gelatine was examined regarding its effect towards modifiable mechanical and rheological characteristics of the ADA-GEL ink (Fig. 1). Various compositions of ADA-GEL were tested regarding optimised printability characteristics. Subsequently, the modified ADA-GEL hydrogels were compared to prior investigated ADA-GEL compositions which had been successfully developed for bio-fabrication as well as scaffold fabrication [11] using printability assessments, nanoindentation, and rheological characterization. To investigate the impact of the thermal pre-treatment of gelatine on a molecular level Fourier-transform infrared spectroscopy (*FTIR*) as well as Sodium dodecyl sulfate-polyacrylamide gel electrophoresis *(SDS-Page)* were conducted.

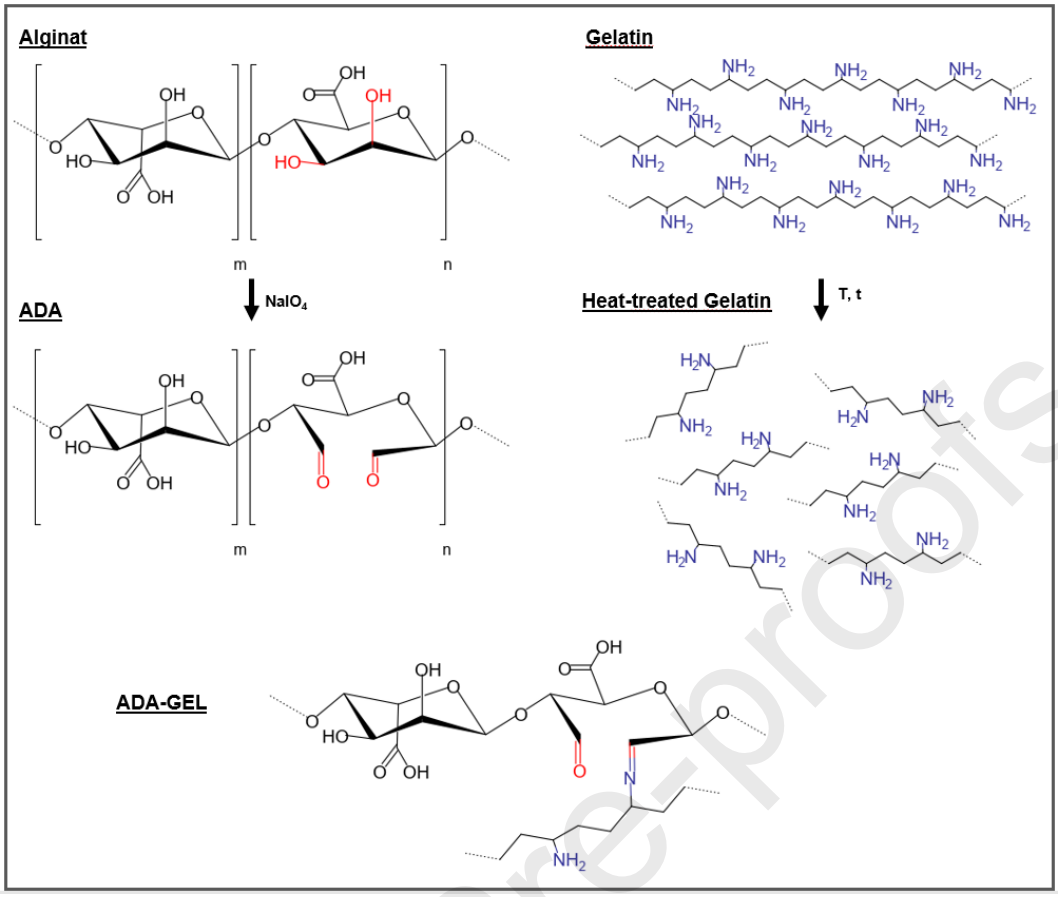

Figure 1: Schematic illustrating the preparation of ADA-GEL.

2. Materials and Methods

2.1 Materials

2.1.1 Material Synthesis (Oxidation of Alginate)

Covalently crosslinked ADA-GEL hydrogel was synthesised as described by Sarker *et al* [20]. Briefly, ADA (*alginate-di-aldehyde*) was prepared by the oxidation of alginate (VIVAPHARM® alginate, PH176, from brown algae, pharmaceutical excipient grade, JRS PHARMA GmbH & Co. KG, Germany) using sodium (meta)periodate ($NaIO_4$, Sigma-Aldrich, Germany) as an oxidising agent in an ethanol-ultrapure water mixture (1:1). The suspension was stirred for 6 h at 22 °C (room temperature, RT) under the complete absence of light. The oxidation reaction was quenched by adding ethylene-glycol (VWR Chemicals International) and stirred for additional 30 minutes. The resultant suspension was transferred into several dialysis molecular porous membrane tubes (MWCO: 6-8 kDa, Spectrum Laboratories, USA) and dialysed against ultrapure water (UPW, Milli-Q®, Merck Millipore, Germany). UPW was changed twice a day during five days of dialysis. After dialysis, the ADA product was frozen for at least 48 hours before it was transferred into the freeze dryer (ALPHA 1-2 LDplus, CHRIST Gefriertrocknungsanlagen, Germany) for lyophilisation.

2.1.2 Biomaterial Ink Formulation

To produce ADA-GEL hydrogel-inks, ADA and gelatine (Type A, derived from porcine skin, gel strength 300, Sigma-Aldrich, Germany) solutions were mixed. For the preparation of 15 wt/vol% gelatine stock solutions, the gelatine was dissolved in UPW at 37, 70, 80 and 95 °C respectively while vigorously stirring for 10 min, 3h or 6 h. All preparations are depicted in Table 1. The warm gelatine solutions were filtered (Carl Roth GmbH&Co. KG, Germany, pore size 0.45 µm) and stored at 4 °C in aliquots for later use. ADA solutions of 7.5 wt/vol% were freshly prepared at the day of their use by stirring in phosphate buffer saline (DPBS) without Ca^{2+}- and Mg^{2+}-content (Gibco® by life technologies™, USA) at RT followed by subsequent filtration (Carl Roth GmbH&Co. KG, Germany, pore size 0.45 µm). For the preparation of the hydrogel-ink, aqueous gelatine solution was slowly added into an ADA solution with a ratio of 1:1 and covalently crosslinked under continuous stirring for 10 min at 37° C. The hydrogels were subsequently ionically crosslinked using 0.1 M $CaCl_2$ and 0.5 M $CaCl_2$ solutions (calcium chloride dihydrate, VWR Chemicals, Germany)

Table 1: Overview of ADA-GEL precursor contents in a not heat-pretreated reference composition (37 °C) in comparison to new formulations.

ADA-GEL formulation	ADA [%w/v]	Gelatine [%w/v]	Pre-treatment Temperatures [°C]	Holding Time
ADA-GEL-T_{Ref}	3.75	3.75	37	10 min
ADA-GEL-$T_{70°C\_6h}$	3.75	7.5	70	6 h
ADA-GEL-$T_{80°C\_3h}$	3.75	7.5	80	3 h
ADA-GEL-$T_{80°C\_6h}$	3.75	7.5	80	6 h
ADA-GEL-$T_{95°C\_3h}$	3.75	7.5	95	3 h

2.2 Material Characterisation

2.2.1 Fourier Transfer Infrared Spectroscopy (FTIR)

An attenuated total reflectance FTIR (ATR-FTIR) spectrophotometer (IRAffinity-1S, Shimadzu, Japan) was used to evaluate the impact of the temperature pre-treatment of gelatine and the crosslinking between ADA and gelatine on the chemical structure. Dried films were used to record ATR-FTIR spectra. Films of gelatine and ADA-GEL were created by casting the corresponding hydrogels into 1.5 ml microtubes (Sarstedt, Germany) and dried for 3 days at RT.

2.2.2 Electrophoretic Analysis

SDS-PAGE was performed to evaluate the impact of thermal pre-treatment on the molecular weight distribution of gelatine. Separating and collecting gels were prepared one day before the experiment. The separating gel was prepared and poured into the sample holder (5 ml) before the polymerization of the solution. It was then polymerized for 1 h. Afterwards, the collecting gel was prepared and added into the sample holder (approx. 1.8 ml) with a further 45 min polymerization step. Gelatine samples were diluted to a protein concentration of 2.3 mg/ml. 15 µl of the sample solution was added to 5 µl loading buffer and mixed extensively. 10 µl blank solution (UPW + buffer) served as. The molecular marker solution (PageRuler™, Thermo Fisher Scientific, US) consisting of 10 defined proteins, was used to estimate the approximate size of the separated protein fragments. 10 µl of the marker and 20 µl of each sample were loaded on their respective lane on the gel. Starting current of 80 V was applied until the samples entered the separating gel in a WAVETETRAD-PP500-system (Cleaver-Scientific, Great Britain). The voltage was then increased to 120 V. The visualisation of the protein bands was performed by using Brilliant Blue R250 staining solution (Thermo Fisher Scientific, US). SDS-PAGE quantification was conducted via Fiji image-J.

2.2.3 Rheological Characterization

Rheological properties of hydrogel-ink formulations were measured using a controlled stress rheometer (DHR-3, TA Instruments, USA) with a 40 mm diameter, cross-hatched geometry to reduce slip of the hydrogel samples. ADA-GEL biomaterial ink- samples were heated up to 37 °C and pipetted onto a temperature-controlled peltier plate held at 25 °C to achieve a homogenous gel distribution. The samples were surrounded by a solvent trap, to avoid dehydration of the hydrogels. Time sweeps were conducted with an angular frequency of 10 rad/s and an oscillatory stress of 0.1 Pa. Amplitude sweeps, frequency sweeps, and recovery sweeps were performed after 20 min of gelation time of the ADA-GEL samples at 25 °C. For amplitude sweeps the angular frequency was set to 10 rad/s. Frequency sweeps were conducted applying an oscillatory stress of 0.1 Pa. Recovery sweeps were carried out with an erratic shear rate increase from 0.01 s^{-1} to 500 s^{-1} after 100 s. The shear rate was decreased to 0.01 s^{-1} after further 100 s to assess the recovery behaviour of the hydrogels. Temperature sweeps were conducted in a temperature range from 20 to 40 °C applying an angular frequency of 10 rad/s and an oscillatory stress of 0.1 Pa.

2.2.4 Nanoindentation

Mechanical testing was performed to determine the effective Young's moduli (E_{eff}) of the hydrogels using a Piuma Nanoindenter (Optics11, Netherlands) equipped with a boro-silicate

glass indenter tip featuring 23 µm radius and 0.47 N/m stiffness (Optics11, Netherlands). Hydrogels were measured in triplicates. Three indentations with 200 µm spacing were performed per hydrogel sample. The median of three indents was taken for every point. Tests were run at RT as well as at 37 °C. ADA-GEL films were deposited in plastic petri dishes and then crosslinked with 0.1 M $CaCl_2$ and 0.5 M $CaCl_2$ for 10 min each. The samples were then rinsed with HBSS (Hank's Balanced Salt Solution, Sigma-Aldrich, Germany), which was subsequently also used as an optical medium during nanoindentation.

2.3 Printability Assessment

Scaffold designs were drafted using the scaffold fabrication software "ScaffoldGenerator" (GeSim GmbH, Germany) as well as G-code and 3D-CAD/CAM-Software Fusion 360 (Autodesk, US). To assess the printability of the hydrogel-inks, single-strand structures and two-dimensional grids were printed using a micro-nozzle with an inner diameter of 410 µm (Nordson Corporation, US). The printing speed was set to 2 mm/s. Air pressures were adapted to the different hydrogel-ink formulations (Table 1) to provide a continuous material flow. Single-strand structures, square two-dimensional grids, and square 3D scaffolds had an edge length of 15 mm. Five struts were plotted over the edge length. The number of layers in z-direction was adapted to the different hydrogel-ink formulations to assess the maximum printable height. Scaffold geometry and structure were analyzed using macroscopic and light microscopy images (Stemi 508, Carl Zeiss Microscopy GmbH, Germany). Image analysis was performed using ImageJ to assess strand thickness, evaluated for n = 10 individual strands, and printing accuracy. The printed areas of square 2D grids with a determined edge length of 15 mm (A_i [mm^2]) were compared to the designed grid area (A = 225 mm^2) to calculate the percentage printing accuracy for each sample using the following equation:

$$Printing\ Accuracy\ (\%) = \left[1 - \frac{|Ai - A|}{A}\right] \times 100 \qquad (1)$$

G-code was written to design a two-dimensional structure to evaluate the possible resolutions of the hydrogel-ink formulations. The distances between strands were varied from 2 mm up to 0.5 mm (Fig. 6 A) in a square structure to assess at which distance strut merging could occur.

A uniformity factor was determined to classify printed strand uniformities and compare them to a theoretically perfect uniform strand [13,21]. For each hydrogel ink, one layer was printed with optimised extrusion pressure and a velocity of 2 mm/s. Each layer was imaged using light microscopy and images were evaluated using ImageJ. The outer edges of three printed strands per hydrogel-ink were outlined and measured. The length was then divided by the length of a theoretical, perfectly uniform strand (straight lines next to the strands) to obtain the uniformity factor U (Eq. 2):

$$U = \frac{length\ of\ printed\ strand}{length\ of\ theoretical\ straight\ strand} \quad (2)$$

Figure 7 H shows a nonuniform (U > 1) and a uniform strand (U = 1) [13]. The pore factor (Pr) was determined to compare printed pores with ideal square pores.

$$\mathrm{Pr} = \frac{(pore\ perimeter)^2}{16\ x\ (pore\ area)} \quad (3)$$

2D-printed hydrogel grids were imaged using a light microscope and evaluated using ImageJ. Three pores were measured (perimeter and pore area) for each hydrogel composition (Table 1) and the pore factor was determined (Eq. 3). A pore factor Pr<1 corresponds to an under-gelled, Pr=1 corresponds to a properly-gelled, and Pr>1 corresponds to an over-gelled material [13].

2.4 Micro Computed Tomography (µ-CT) analysis

X-ray computed tomography (CT) measurements were performed using the "CTportable160.90" device developed by the Development Center X-Ray Technology (EZRT) of the Fraunhofer Institute (Fürth, Germany). The system was operated at 60 kV and 120 µA and a nominal spatial voxel sampling of 24.23 µm to cover the whole sample diameter during the scan (Focus object distance of 93 mm, focus detector distance of 190 mm). A total of 800 projections within one 360° rotation in a FlyBy acquisition were taken with an exposure time of 200 ms. The FlyBy acquisition procedure rotates the object constantly during the image exposure and resulted in measurement times of 2,6 min. The software used for data acquisition was Volex 10 (Fraunhofer EZRT, Germany). All images were 3D reconstructed with a filtered back-projection algorithm (Fraunhofer EZRT, Germany, REL-2.1.1) and afterwards analysed with the BlobAnalysis algorithm from Fraunhofer EZRT. The BlobAnalysis algorithm utilizes an image segmentation chain on multiple watersheds and morphological operations and calculates the number of voxels in the pore, the centre of mass of the pore in x,y,z coordinates, the aspect ratio, and the normalized pore diameter for each detected pore.

2.5 Statistical Analysis

Data are expressed as mean ± standard deviation (SD). Statistical analysis was performed using Origin2016G software (OriginLab Corporation, USA). All experiments were performed using a minimum of n = 3 replicates. Normality tests and analysis of variance homogeneity were performed using the Shapiro-Wilk test. Statistically significant differences between

means were determined at a value of $p < 0.05$, as determined by the Bonferroni post-hoc test using one-way analysis of variances (ANOVA) testing. Different significance levels (p-values) are indicated with asterisks and the specific p-value is provided in each figure legend.

3. Results & Discussion

3.1 Denaturation of Gelatine via Heat Treatment

Temperature pre-treated gelatine was examined via FTIR to gather structural information and data about intra- and intermolecular dependencies (Fig. 2). The FTIR spectra of pre-treated gelatines showed characteristic absorption bands of polypeptides and proteins including amide I (~ 1635 cm^{-1}), amide II (~ 1527 cm^{-1}) and amide III bands (~ 1238 cm^{-1}), caused by amide bonds linking amino acids. Amide I bands are induced by C=O stretching whereas amide II is caused by bending vibrations of N–H groups and stretching vibrations of C–N groups. Amide III is related to the vibrations in the plane of C–N and N–H groups of bound amide [22–24].

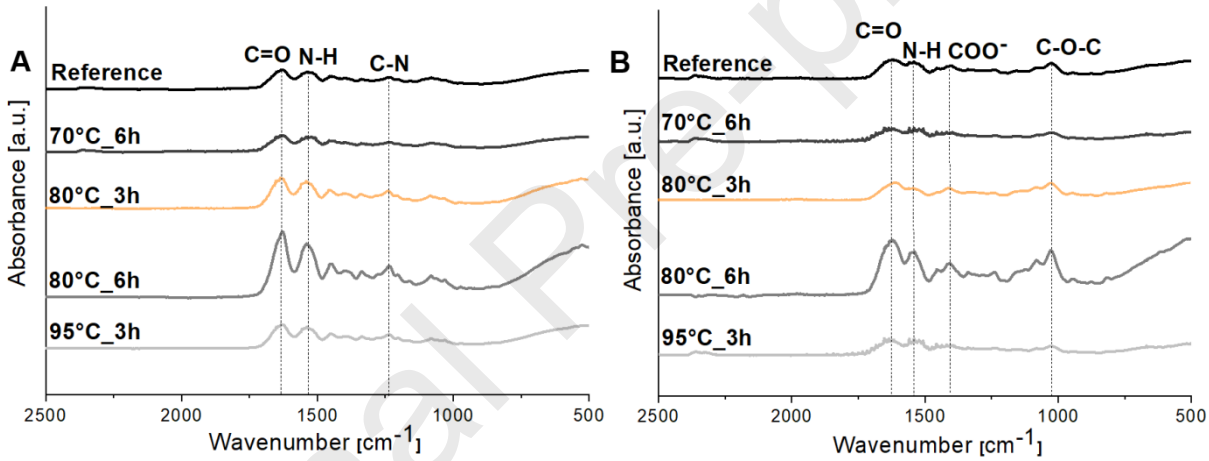

Figure 2: FTIR analysis of heat pre-treated gelatine and corresponding ADA-GELs. **A:** FTIR spectra of heat-treated gelatine (Type A, bloom 300) treated for 3 h and 6 h at 70, 80, and 95 °C. The gelatine reference was dissolved at 37 °C. **B:** FTIR spectra of ADA-GEL composed of oxidized alginate and pre-treated gelatines.

All samples modified by the heating pre-treatment showed no changes in wavenumbers for amide I, amide II and amide III peak positions indicating an intact primary protein structure of gelatine. In contrast to the gelatine spectra, ADA-GEL spectra featured extra peaks which are residues of the alginate at 1027 cm^{-1} due to C-O-C stretching and at 1408 cm^{-1} due to asymmetric COO^- stretching [25]. Amide I (1625 cm^{-1}) and II (1538 cm^{-1}) bands shifted and broadened indicating the additional formation of C=N bonds absorbing at 1538 cm^{-1} which is a sign of Schiff's base formation and therefore covalent crosslinking of ADA and gelatine [26]. However, amide III bands could hardly be seen most likely due to overlapping signals of gelatine and ADA. Yet, the pre-treatment of gelatine precursor solutions showed no changes in the wavenumbers of the ADA-GEL spectra indicating the unaltered structure of amide I and II motifs contributing to the Schiff's base formation with the aldehyde groups of ADA. Unaltered

amide I and II motifs were also obtained by FTIR analysis by Hoque et al. examining the thermal treatment of cuttlefish skin gelatine [27]. In conclusion, from the FTIR study, it was hypothesized that a temperature increase firstly manipulates the tertiary and secondary protein structure leading to an irreversible denaturation upon further heating [28]. Intramolecular hydrogen bonds are broken by the heat treatment and substituted with hydrogen bonds to water molecules which prohibit the reformation of the native tertiary protein conformation [28]. Nonetheless, FTIR results indicate an intact primary structure of gelatine independent of the dissolution temperature, allowing the formation of covalent crosslinks between oxidized alginate and gelatine via Schiff's base formation, as described before [29]. The electrophoresis patterns of heat pre-treated gelatines (protein concentration of 2.3 mg/ml) are shown in Fig. 3 A. Gelatine dissolved at 37 °C served as control. The molecular weight distribution fitted the manufacturers' specification of approximately 100 kDa [30].

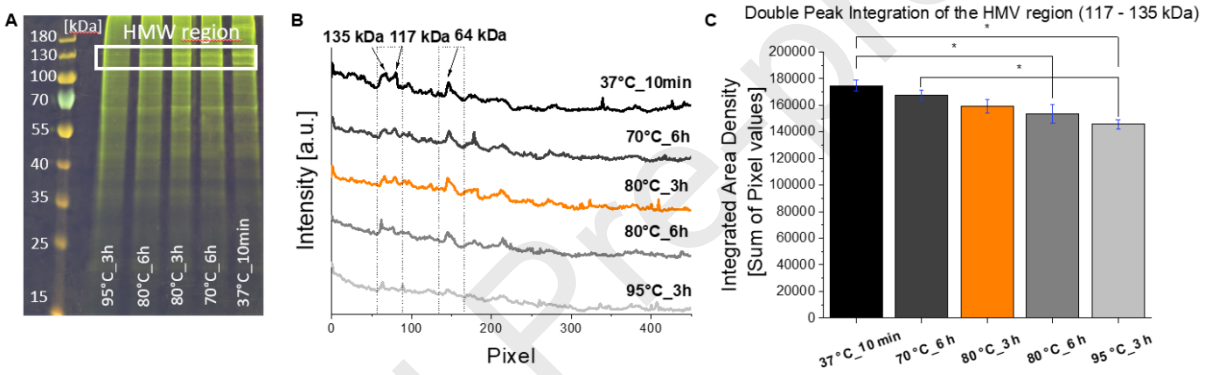

Figure 3: SDS-PAGE of temperature pre-treated gelatines. **A:** Protein pattern. Each lane represents a different temperature pre-treatment of gelatine (reducing temperature from left to right). **B:** Corresponding intensity spectra of temperature pre-treated gelatines derived from the protein pattern. **C:** Area intensity integration of the marked high molecular weight (HMW) region. Data are shown as mean ± SD. *p < 0.05. Statistical differences of means were analysed using one-way ANOVA.

The most abundant protein molecular weights were found to be at 135, 117 and 64 kDa. Heat-treated gelatine solutions were degraded which could be seen in washed-out protein bands in a range of 40 – 180 kDa. Furthermore, additional protein bands appeared in lower molecular weight regions (< 40 kDa). This effect intensified with increasing dissolution temperatures of gelatine with the most severe effect at a pre-treatment at 95 °C for 3 h. These observations could be confirmed via a comparison of the intensity spectra of each protein band (Fig. 3 B). Intensities in high molecular weight regions (> 55 kDa) decreased with increasing pre-treatment temperatures and holding times. This indicated a decrease in large molecular weight molecules and therefore a degradation of gelatine. Due to the absence of enzymes, the main factor for degradation was identified as hydrolysis due to the temperature treatment during the preparation of the gelatine solutions. Similar results were achieved by Hoque *et al* [27]. Cuttlefish skin gelatine was heat-treated for 30 min at 40, 50, 60, 70, 80, and 90 °C. It was

observed that gelatine degradation occurred using heat treatments higher than 70 °C [27]. In addition to incubation time and temperature, Van den Bosch *et al.* proved that gelatine concentration and solvent (type and concentration of salt ions and pH) have an additional impact on gelatine degradation [31]. In this work, gelatines with concentrations of 15 %(w/v) were used for temperature pre-treatment in the absence of additional ions. In summary, SDS–PAGE revealed that gelatine was susceptible to degradation due to the pre-treatment at elevated temperatures. Hence, it could be assumed that a pre-treatment of gelatine would allow a possible tunability of material characteristics.

3.2 Rheological Assessment

Rheological measurements were performed to determine the time-dependent viscosity, yield stress, shear rate-dependent viscosity, temperature-dependent viscosity, and the recovery behaviour of the chosen hydrogels (Fig 4). ADA-GEL hydrogel precursors were formed via mixing at 37 °C. Since all bioprinting procedures were performed at RT, a gelation process of the gelatine occurred due to the cooling-off. Hence, a time-sweep was carried out to evaluate after which time a hydrogel-ink could be considered printable. The complex viscosities of the ADA-GEL increased over time reaching a plateau region eventually (Fig.4 A). This could be attributed to the gelling of ADA-GELs during cooling. Initially, isolated colloidal aggregates, which were present in the suspension, crosslinked to form a 3D, highly-viscous network [32]. Thus, the progress of complex viscosity over time depended on polymer concentration and degree of polymer denaturation (Fig. 4 A). Similar results were found by Ouyang et al [33]. It was shown that an increased gelatine concentration increased the viscosity of an alginate gelatine blend (x % gelatine + 1 % alginate). Consequently, the degree of thermally modified gelatine led to an altered molecular distribution, as confirmed via SDS-PAGE. This was due to physical entanglements in the polymer solution. Despite no actual crosslinking in the solution, those entanglements and overlapping polymer chains interacted as a viscous network. The results indicate that at higher concentrations, the probability of chain interactions (entanglements and rearrangements) was higher than in less concentrated solutions, which led to an increase of viscosity [34]. Consequently, ADA-GEL-$T_{80°C\_6h}$ and ADA-GEL-$T_{95°C\_3h}$ featured lower viscosities over time compared to the ADA-GEL-T_{Ref} despite higher gelatine concentrations but due to higher degrees of thermal denaturation (Fig. 3). ADA-GEL-$T_{80°C\_3h}$ presented the highest viscosities over time due to a high gelatine concentration in comparison to the ADA-GEL-T_{Ref} and low thermal denaturation in comparison to the other ADA-GELs with a higher content of thermally-modified gelatine. Since cell viabilities of possibly encapsulated cells for potential further applications were kept in mind, a gelation time of 20 min at RT was chosen for further rheological experiments. This was done to account for viscosities that would allow proper printing (Fig. 4 A) and to minimize the time at which cells would be exposed to a

potentially harmful and not ideal temperature (22 °C). Considering the time-sweep, the especially well-fitting hydrogel formulations meeting this demand could be determined via a visualisation approach. Fig. 4 F depicts a bottle flip test to assess gelation of the hydrogels at reduced temperatures (RT). ADA-GEL-$T_{70°C\_6h}$ and ADA-GEL-$T_{80°C\_3h}$ could exclusively defy gravity, firstly after 20 min in comparison to other compositions. The result proved that after a certain time point of the ADA-GEL gelation process additional yield stress would be required to trigger material flow. However, after 20 min, gelling continued what resulted in higher viscosities for the ADA-GELs (Fig. 4 F). Hence, the results indicated that printing pressures had to be adjusted during continuous printing.

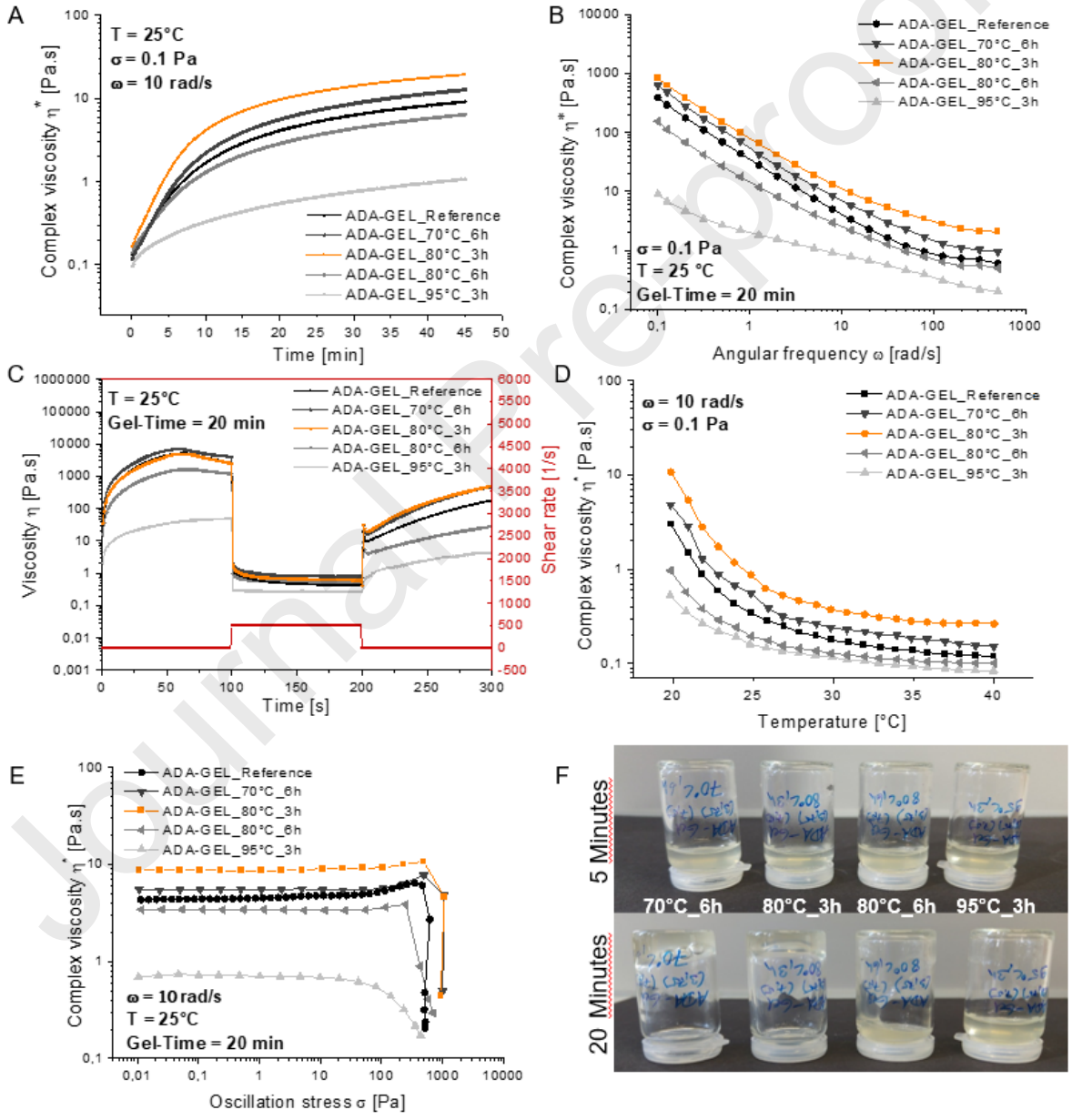

Figure 4: Rheological assessment. **A:** Time-dependent change of complex viscosities for the selected ADA-GEL samples. Tests were performed with an angular frequency of 10 rad/s and an oscillation stress of 0.1 Pa over a time of 45 min at 25 °C. **B:** Frequency-dependent change of complex viscosity illustrating the shear-thinning

behaviour of the ADA-GELs. Tests were performed with oscillatory stress of 0.1 Pa after 20 min of gelling time at 25 °C. **C:** Shear rate triggered recovery behaviour of ADA-GEL viscosities. The experiments were performed after a gelling time of 20 min at 25 °C. **D:** Temperature-dependent change of complex viscosity illustrating the gelation behaviour of ADA-GELs at lower temperatures. Tests were performed with an angular frequency of 10 rad/s and oscillatory stress of 0.1 Pa. **E:** Stress-dependent change of complex viscosity revealing the starting point of material flow, known as the yield stress. Tests were performed with an angular frequency of 10 rad/s after 20 min of gelling time at 25 °C. **F:** Visualized rheological behaviour of modified ADA-GELs cooling down from 37 °C after 5 min and after 20 min. Left: ADA-GEL-$T_{70°C\_6h}$. Second from left: ADA-GEL-$T_{80°C\_3h}$. Second from right: ADA-GEL-$T_{80°C\_6h}$. Right: ADA-GEL-$T_{95°C\_3h}$.

The yield stress plays an important role in hydrogel-ink formulations since it defines the shear stress for material flow initiation. Fig. 4 E depicts the shear stress ramps of the ADA-GELs. Shear stress ramps allowed the characterisation of the yield stress of the material, below which the material behaved rather like a solid than like a liquid. Highest yield stresses were found with ADA-GEL-$T_{80°C\_3h}$ (489.7 Pa) and ADA-GEL-$T_{70°C\_6h}$ (489.4 Pa) followed by ADA-GEL-T_{Ref} (345.9 Pa), ADA-GEL-$T_{80°C\_6h}$ (248.2 Pa), and ADA-GEL-$T_{95°C\_3h}$ (140.1 Pa). ADA-GEL-$T_{80°C\_6h}$ and ADA-GEL-$T_{95°C\_3h}$ exhibited much lower yield stresses indicating the impact of precursor modification and its role in the improvement of the rheological properties for hydrogel printability. Additionally, 70°C_6h and 80°C_3h samples demonstrated significantly higher yield stress points than the other compositions (Fig. 4 E + SI Table 5). Paxton et al. determined the yield stress of 20 wt% poloxamer 407 (93.6 Pa), 25 wt% poloxamer 407 (227 Pa), 30 wt% poloxamer 407 (348 Pa), Nivea Crème (72.1 Pa), and from 8 % w/v / 1 % w/v alginate-gelatine blend (166 Pa) [35]. Yield stresses were found to have similar orders of magnitude. Compared to Paxton et al. [35], however, ADA-GEL-$T_{80°C\_3h}$ and ADA-GEL-$T_{70°C\_6h}$ featured higher yield stresses. Yield stresses of ADA-GEL-T_{Ref} and 30 wt% poloxamer 407 were similar. Just as with 8 % w/v / 1 % w/v alginate gelatine blend and ADA-GEL-$T_{95°C\_3h}$. It was observed that the yield point viscosities for ADA-GEL-$T_{70°C\_6h}$ and ADA-GEL-$T_{80°C\_3h}$ were above 5 Pa.s and therefore significantly higher than for the other formulations. Moreover, all samples showed a shear-thinning behaviour, characterised by a decrease in complex viscosity over an increasing shear rate (Fig. 4 B). Information about shear thinning is crucial for the printability of hydrogels since it is responsible for a smooth material extrusion without clogging [36]. ADA-GEL-$T_{95°C\_3h}$ exhibited significantly lower viscosities over the shear rate ramp compared to the other ADA-GELs. Viscosity values of ADA-GELs were in accordance with the gelatine concentration and degree of denaturation used in the ADA-GEL hydrogel, with ADA-GEL-$T_{80°C\_3h}$ featuring the highest viscosities in the examined frequency spectrum. In theory, shear-thinning of the ADA-GELs could be caused by disentanglements of polymer chains during flow. Hence, when sheared, ADA-GELs would disentangle and aligned which would cause the viscosity to drop. The degree of disentanglement depended on the shear rate. At sufficiently high shear rates the polymer chains could be completely disentangled and fully aligned. In this range, the

viscosity would be independent of the shear rate featuring plateau-like regions like it was seen for each ADA-GEL sample (Fig. 4 B) [37]. The recovery behaviour of hydrogel inks was especially important for the post-printing behaviour of each printed strand. Physically, recovery allows the material to rapidly increase in viscosity after extrusion and to maintain a high shape fidelity [35]. Figure 4 C shows the recovery results for the ADA-GEL compositions. ADA-GEL-$T_{70°C\_6h}$, as well as ADA-GEL-$T_{80°C\_3h}$, showed the fastest recoveries after application of the high shear rate compared to the ADA-GEL-T_{Ref}. This could also be attributed to the higher content of gelatine in comparison to ADA-GEL-T_{Ref}. Despite the gelatine denaturation, the higher polymer concentrations could lead to more interactions and entanglements between the polymer chains. By comparison, ADA-GEL-$T_{95°C\_3h}$ showed the worst recovery behaviour due to the highest gelatine denaturation by the temperature treatment, proving its impracticality for further printing. However, all ADA-GEL hydrogels were not able to fully recover in the following 100 s after extrusion (Fig. 4 E). In general, longer recovery times led to a decrease in the retention of cylindrical fibre formation and shape fidelity (Fig. 6 E). To achieve printability improvements, the ADA concentration could be increased to gain a denser polymer network with more possibilities for entanglements and therefore faster recoveries. Temperature sweeps were conducted to characterise the thermoresponsive properties of the ADA-GELs. Thermoresponsivity could be employed to cause changes in viscoelastic properties required for successful extrusion and solidification into 3D constructs with high shape fidelity after printing. Thermo-responsivity was characterised by a change in a material's viscoelastic properties as a result of temperature change (Fig. 4 D). During bioprinting, temperature enables the control of the hydrogel viscosity. An increase of viscosities could be seen for all ADA-GELs upon cooling (Fig. 4 D, ramp from 40 °C to 20 °C), due to increasing entanglements and alignments of polymer chains trying to restore their natural conformation upon cooling. Hence, initially isolated colloidal aggregates present in suspension crosslinked to form a three-dimensional, viscoelastic network featuring higher viscosities [38]. Since the temperature sweeps were conducted by cooling from 40 °C to 20 °C viscosity values at 25 °C appeared relatively low in comparison to other sweeps since gelation still had to take place. Regarding biofabrication, previous studies have shown that adding high cell numbers (> four million/ml-1) significantly reduces final ADA-GEL hydrogel stiffness [39]. It has been shown for a gelatin-based hydrogel that increasing cell concentration reduces bioink viscosity [40]. As a result, those studies imply that our biomaterial ink may show reduced viscosity for high cell numbers, which may impact the printability and rheological properties of the here presented hydrogel composition. In this study, we focused on the engineering and design of an ADA-GEL composition with increased printability to produce biomaterial scaffolds that do not contain cells. In future studies, we will assess the influence of higher cell concentrations on the final

hydrogel rheological properties, which will provide important implications for future biofabricaton approaches with the here presented, optimized ADA-GEL matrix.

3.3 Nanoindentation

Fig. 5 shows the effective Young's modulus of ADA-GEL samples crosslinked with 0.1 M and 0.5 M $CaCl_2$ for 10 min. Samples measured at RT and 37 °C were compared. At 37 °C, the effective Young's moduli were significantly lower than at RT for all ADA-GEL samples. This decrease in the stiffness could be explained by the fact that gelatine is a thermo-reversible gel featuring a characteristic melting point of 37 °C [41]. Hence, the greater the gelatine content in the ADA-GEL, the greater the impact of temperature increase. ADA-GEL-T_{Ref} showed a smaller drop in stiffness. This could be attributed to the degree of crosslinking between ADA and gelatine, which is dependent on GEL-to-ADA ratio. Sarker *et al.* reported that a high crosslinking degree of ADA-GEL with lower gelatine content can be explained by the availability of more reactive aldehyde groups of ADA. High ADA content could promote the extent of crosslinking with the free amino groups of gelatine [20]. In contrast, ADA-GEL compositions with high gelatine content had comparatively lesser amounts of reactive aldehyde groups for crosslinking [29]. In conclusion, the combination of concentration, the degree of crosslinking and Ca^{2+} gelation influenced the mechanical properties of the ADA-GEL system. Calcium-induced gelation has been demonstrated to result from specific and strong interactions between calcium ions and guluronate blocks in alginate, respectively. Hence, increased $CaCl_2$ concentrations led to slightly higher effective Young's moduli. This result is in agreement with the results of Remunan-Lopez *et al.* who described increasing mechanical properties of alginate as a function of increasing $CaCl_2$ concentrations [42]. Corresponding to strong gelatine denaturation, ADA-GEL-$T_{80°C\_6h}$ and ADA-GEL-$T_{95°C\_3h}$ exhibited lower stiffness values and stronger stiffness drops at 37 °C compared to the ADA-GEL-T_{Ref}, despite higher gelatine concentrations. ADA-GEL-$T_{80°\_3h}$ and ADA-GEL-$T_{70°C\_6h}$, however, exhibited lower degrees of degradation which resulted in similar stiffness values compared to the ADA-GEL-T_{Ref} due to the additional gelatine concentration [41]. Compared to the results of Zehnder *et al.* [11], significantly lower stiffness values were achieved in this work despite the same composition (ADA-GEL-T_{Ref}), the same crosslinking agent as well as the same crosslinking time. The only difference was the source of alginate. A possible reason could be that Zehnder *et al.* used sodium alginate with a high guluronic acid content of 65 % – 70 %. It is known that calcium primary cross-links the guluronic residues. Because of high guluronic acid contents in the alginate, the gel strength could be dramatically increased [43]. Since in this work alginate was changed to GRINDSTED® Alginate PH 176 featuring a molecular weight of 250000 g/mol but unknown guluronic acid/ mannuronic acid ratio, it was considered that this alginate had a significantly lower guluronic acid content, which could result in lower Young's moduli. Studies

have shown clear correlations between elastic moduli of hydrogel matrices and proliferation as well as differentiation of encapsulated cells [44].

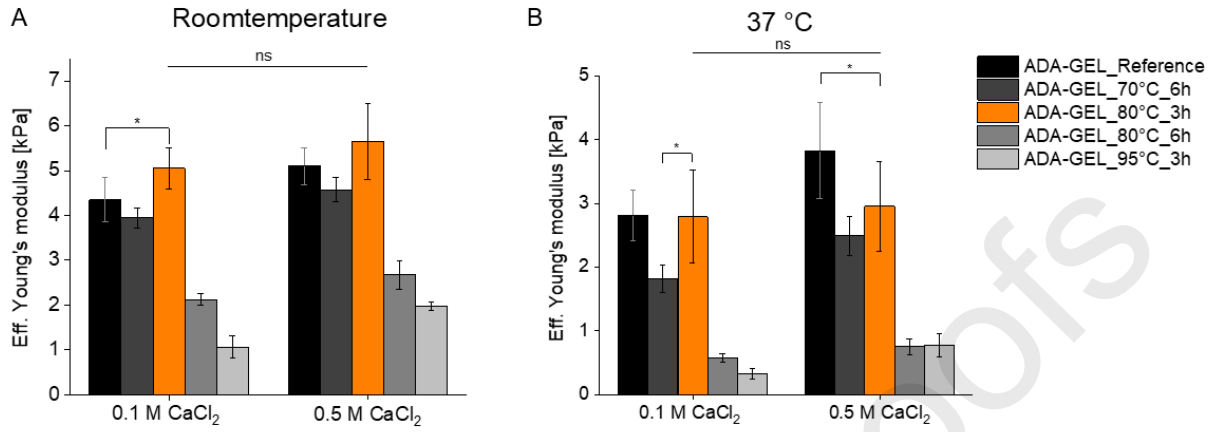

Figure 5: Effective Young's moduli of ADA–GEL samples crosslinked with 0.1 M and 0.5 M $CaCl_2$ measured at **A:** room temperature (RT) and **B:** 37 °C. The asterisks indicate differences with $p < 0.05$ obtained from Bonferroni test.

Yet, Zehnder *et al.* [11] followed a bone tissue engineering approach in contrast to this work which made higher moduli necessary for a suitable bone cell environment. The elastic modulus of mammalian chondral tissue (matrix around chondrocytes) (~ 25 ± 5 kPa), however, is lower than the one of bone (cortical bone ~ 15 ± 5 GPa) [45,46]. In comparison to these values, elastic moduli of ADA-GEL samples crosslinked with $CaCl_2$ are in the range of soft tissue elastic moduli (~ 4 ± 2 kPa) [45]. This indicates a suitable environment for cell encapsulation for cartilage tissue engineering since both matrix stiffness and composition are important for the retention of tissue-specific cell functionality [47]. However, the optimal value of the elastic modulus may depend on the cell type.

3.4 Printability

Heat pre-treatment of gelatine solutions significantly affected the printability of ADA-GEL formulations. These formulations were evaluated regarding printing accuracy, strand width, resolution, printing pressure, uniformity factor (U), pore factor (Pr), gelation times, and shape stability as well as fidelity in the z-direction. The material selection of ADA-GELs showed printing accuracies of over 90 % with slightly higher values compared to the ADA-GEL-T_{Ref} due to the higher concentrations of modified gelatine which led to a greater amount of polymer chain interactions like entanglements and crosslinks in the hydrogel (Fig. 7 A). Due to higher degrees of degradation gelatines dissolved at higher temperatures led to smoother strand appearances (Fig. 6). A smoother strand appearance of an ADA-GEL with highly denatured gelatine content could be expected (Fig. 6 D) since gels of lower viscosities showed a more

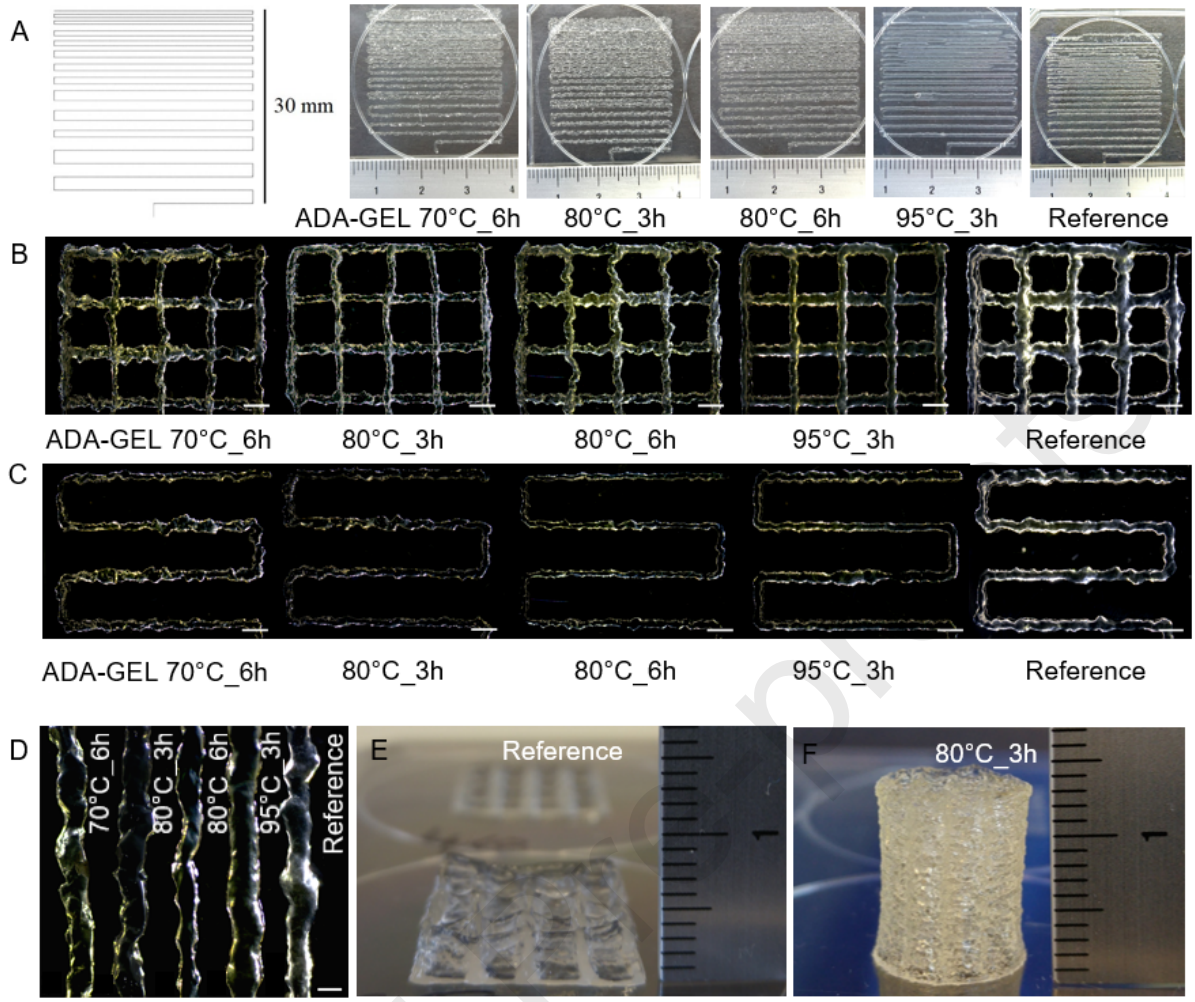

Figure 6: Printability assessment. **A:** Resolution structures. From left to right: CAD-File, ADA-GEL-$T_{70°C\_6h}$, ADA-GEL-$T_{80°C\_3h}$, ADA-GEL-$T_{80°C\_6h}$, ADA-GEL-$T_{95°C\_3h}$, ADA-GEL-T_{Ref}. **B:** 3D printed ADA-GEL-Grids. From left to right: ADA-GEL-$T_{70°C\_6h}$, ADA-GEL-$T_{80°C\_3h}$, ADA-GEL-$T_{80°C\_6h}$, ADA-GEL-$T_{95°C\_3h}$, ADA-GEL-T_{Ref}, Scale: 2000 µm. **C:** 3D printed ADA-GEL-Single-Layer. From left to right: ADA-GEL-$T_{70°C\_6h}$, ADA-GEL-$T_{80°C\_3h}$, ADA-GEL-$T_{80°C\_6h}$, ADA-GEL-$T_{95°C\_3h}$, ADA-GEL-T_{Ref}, Scale: 2000 µm. **D:** 3D printed ADA-GEL-Strands. From left to right: ADA-GEL-$T_{70°C\_6h}$, ADA-GEL-$T_{80°C\_3h}$, ADA-GEL-$T_{80°C\_6h}$, ADA-GEL-$T_{95°C\_3h}$, ADA-GEL-T_{Ref}, Scale: 500 µm. **E:** Obtainable height stability using ADA-GEL-T_{Ref}. **F:** Obtainable height stability using ADA-GEL-$T_{80°C\_3h}$.

fluid-like behaviour and broadened strands due to a less dense polymer network and fewer entanglements of polymer chains [48]. The thinnest strands of approximately 0.52 mm were printed with formulations of ADA-GEL-$T_{70°C\_6h}$ and ADA-GEL-$T_{80\ °C\_3h}$. By using a precision tip needle with an inner diameter of 0.41 mm, the logical consequence was that the thinnest possible strand matched this exact value. The thinnest strands observed were 29 % larger than this inner diameter. However, this width increase could be expected due to gravity and surface energy and tension [49]. Increases of strand diameters in 3D structures could be further explained by the additional weight of the higher layers. Resolutions (= required strand distances to avoid merging strands) were determined using self-designed printed resolution structures (Fig. 6 A). Resolution structures supported the results of strand widths and

accuracies. ADA-GEL-$T_{80°C\_3h}$ featured the lowest possible distances between printed strands (≈ 0.68 mm) to avoid strand merging in the same layer with significant differences to ADA-GEL-$T_{80°C\_6h}$, ADA-GEL-$T_{95°C\_3h}$, ADA-GEL-T_{Ref}. Low viscous ADA-GELs with high denatured gelatine content further led to higher gelation times and lower printing pressures (Fig. 7 D+G). Since encapsulated cells in hydrogel-inks experience shear forces during the printing process, lower printing pressures could be favourable [50]. The comparatively low printing pressure of the reference composition might be traced back to its lesser content of not pre-treated gelatine. No significant differences (0.05 level) were found comparing the uniformity factors of the examined ADA-GELs (Fig. 7 E). Uniformity factors (U) ranged from 1.02 to 1.08 showing only slight deviations from a perfectly uniform strand (U = 1).

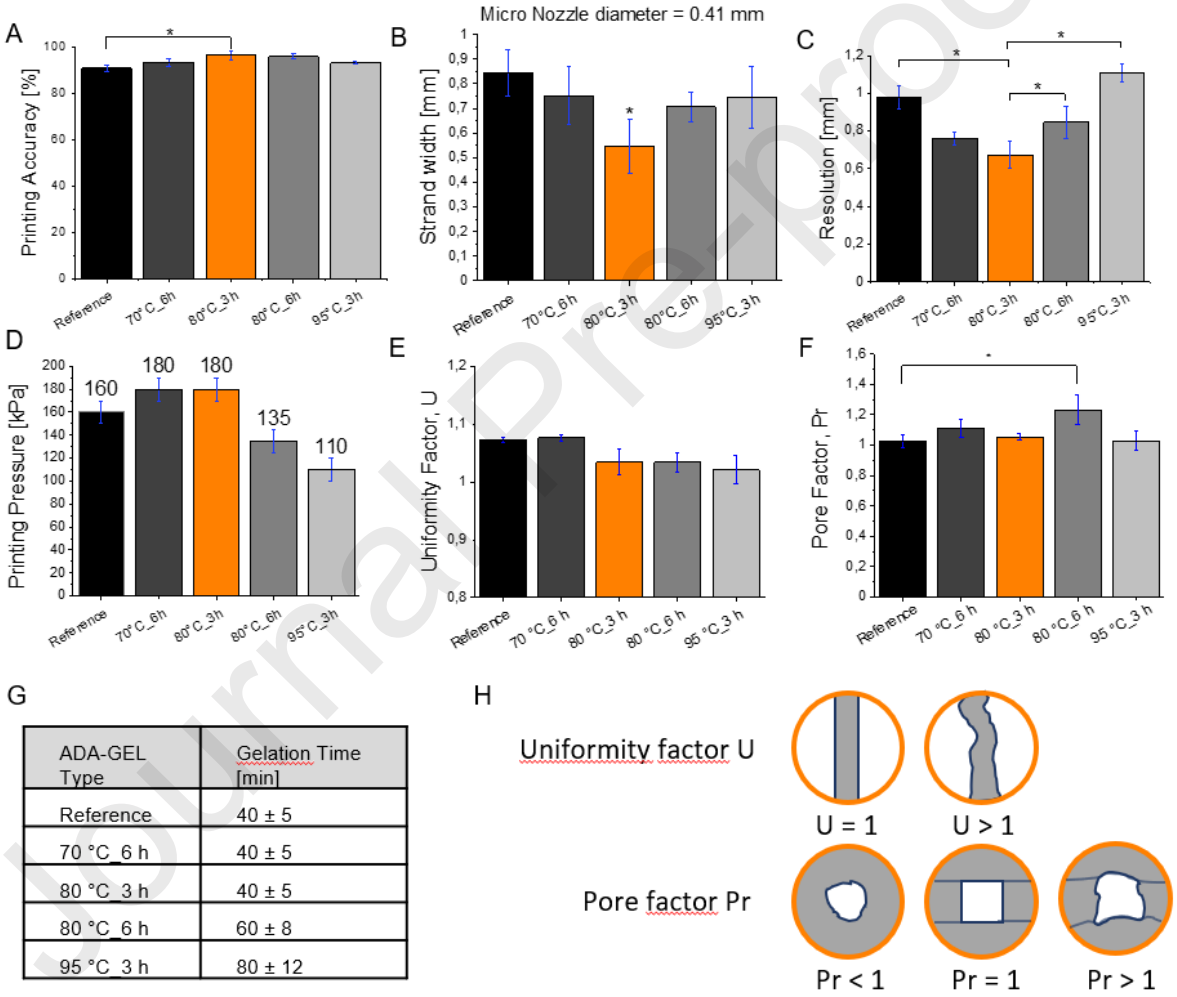

ADA-GEL Type	Gelation Time [min]
Reference	40 ± 5
70 °C_6 h	40 ± 5
80 °C_3 h	40 ± 5
80 °C_6 h	60 ± 8
95 °C_3 h	80 ± 12

Figure 7: Printability evaluation. **A:** Printing accuracies derived from ADA-GEL-Grids. **B:** Strand width comparison. **C:** Resolutions (= Required strand distances to avoid merging strands). **D:** Printing pressures. **E:** Uniformity factor comparison. **F:** Pore factor comparison. **G:** Gelation times before 3D printing is possible. **H:** Schematic of uniformity (U) and pore (Pr) factor ranges (redesigned from Soltan et al. [13]). The asterisks indicate significant differences with $p < 0.05$ obtained from Bonferroni test.

The best uniformity factors (comparing average values) could be achieved with ADA-GEL-$T_{80°C\_3h}$ (1.03 ± 0.02), ADA-GEL-$T_{80°C\_6h}$ (1.03 ± 0.02), and ADA-GEL-$T_{95°C\_3h}$ (1.02 ± 0.02) followed by ADA-GEL-T_{Ref} (1.07 ± 0.01) and ADA-GEL-$T_{70°C\_6h}$ (1.08 ± 0.01). Compared to Soltan et al. [13] slightly higher uniformity factors were found in this work. This result could be explained with an overall higher final concentration of ADA and gelatine, as well as higher printing pressures in combination with lower printing speeds (2 mm/s compared to 25 mm/s). ADA-GELs with gelatine content heat pre-treated at 80 and 95 °C exhibited mean uniformity values which were closest to a perfect uniform strand (Fig. 7 E). This result is in accordance with the qualitative uniformity comparison of heat pre-treated 3D printed gelatine strands of Kolesky et al [51]. Gelatine heat-treated at 95 °C was shown to exhibit more uniform strands after 3D printing than gelatine heat-treated at 70 °C. Pore factors (Pr) ranged from 1.02 to 1.23. These factors are close to a perfectly-gelled hydrogel-ink (Pr = 1) with slight tendencies to an over-gelled material (Pr > 1). Best results could be achieved with ADA-GEL-$T_{80°C\_3h}$ (1.05 ± 0.02), ADA-GEL-$T_{95°C\_3h}$ (1.03 ± 0.06) and ADA-GEL-T_{Ref} (1.02 ± 0.05) followed by ADA-GEL-$T_{70°C\_6h}$ (1.11 ± 0.06) and ADA-GEL-$T_{80°C\_6h}$ (1.23 ± 0.1). Compared to the results of Soltan et al. [13], pore factors were closer to 1. Soltan et al. [13] reported a mainly under-gelled ADA-GEL behaviour most likely due to lower final concentrations of ADA and gelatine as well as no rheological tunability using gelatine denaturation. To assess shape stability and fidelity in higher layers, high multilayer structures were printed. Only ADA-GEL-$T_{80°C\_3h}$ provided the necessary shape stability to maintain its structure throughout the whole printing process of over 50 layers achieving heights of over 1 cm (Fig. 6 F). Gelatines treated at 80°C for 6 h or in general at 95 °C resulted in formulations with deficient viscosity to achieve scaffolds with a sufficient height or stability. This was an expectable result since already the 2D grids featured a fluidic behaviour expressed by thick and merging strands which prohibited shape stability and layer stacking (Fig. 6 A-D). After the evaluation and consideration of all requirements, ADA-GEL-$T_{80°C\_3h}$ was found to possess the best printing characteristics. In comparison to the reference ADA-GEL composition of Zehnder et al. [11], higher printing accuracies, better resolution and higher shape stability could be achieved by composition adjustments as well as structural modifications of the precursors. Hydrogel ink development as well as printing parameter adjustments were the crucial first steps to enable hierarchical 3D printing as a biomimicry approach towards cartilage tissue engineering. The first approach for hierarchical printing was the creation of a scaffold featuring layers with varying densities from bottom to top. Furthermore, to overcome the usual layer stacking approach of 3D plotting a programme was written via G-code. The G-code enabled hydrogel extrusion during a print-head movement in z-direction. Hence, a standard scaffold structure was printed on a dense bottom layer to support vertically printed pillars (Fig. 8 C+D). The dense bottom layer resembles the superficial zone whereas the pillars mimic the deep zone of natural cartilage tissue (Fig. 8 E).

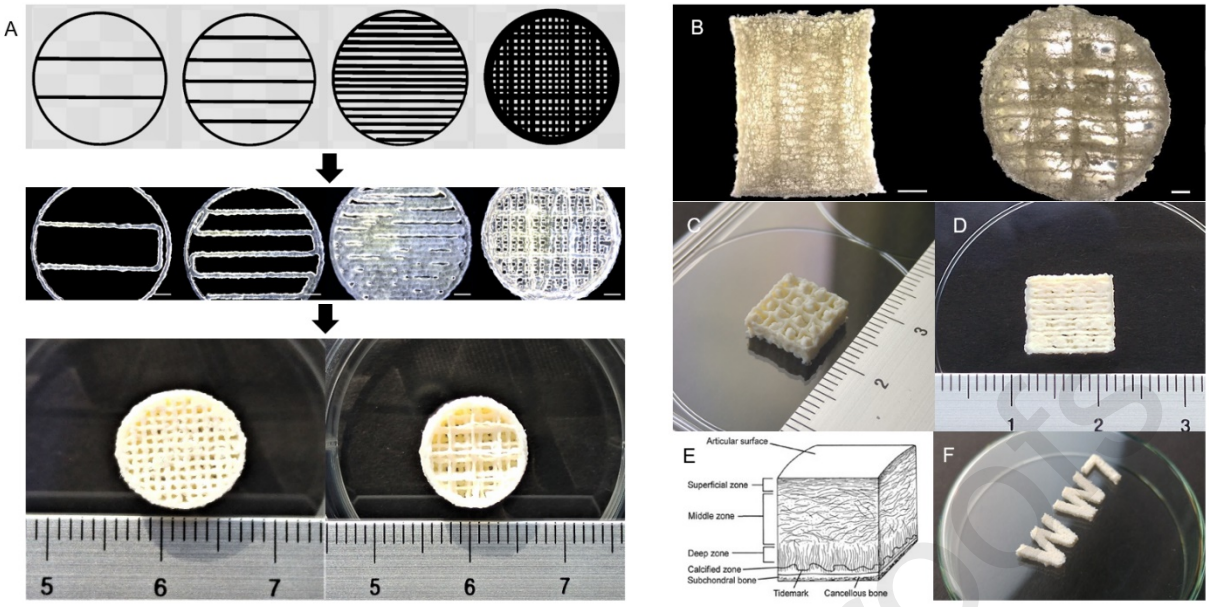

Figure 8: ADA-GEL-$T_{80°C\_3h}$ scaffolds. **A:** Hierarchical scaffold development **Top:** CAD-Files of single layers which are stacked for a 3D hierarchical print forming a hierarchical scaffold with density gradient (Top right). **Center:** 3D print execution. Scale: 2 mm. **Bottom:** Critical point dried hierarchical scaffold. **Left:** Bottom view. **Right:** Top view. **B:** Freeze-dried scaffold as a result of shape stability testing in higher layers. **Left:** Side View. Scale: 2 mm. **Right:** Bottom view. Scale: 1 mm. **C:** Critical point dried hierarchical scaffold as a biomimetic approach towards cartilage tissue featuring pillars printed in the Z-direction. **D:** Bottom view, biomimetic approach. **E:** Structure of natural cartilage tissue [2]. **F:** Institute of Biomaterials Erlangen logo (WW7) 3D printed with ADA-GEL-$T_{80°C\_3h}$ and critical point dried.

µ-CT analysis revealed the micro- and macroporous structures of critical point dried 3D printed ADA-$GEL_{80°C\_3h}$ scaffolds throughout XY (top view) and XZ (side view) planes (Fig. 9). The comparison of µ-CT images of various XY and XZ planes of a scaffold offered information about its porosity gradient. In this work, µ-CT data of a scaffold reference with consistent strut density was compared to the three-layered hierarchical scaffold (Fig. 9 A+B). Despite its homogeneous design, the reference cylinder featured a heterogeneous porosity gradient. Comparing its upper XY 130 plane with the subjacent XY 180 plane it becomes apparent that lower layers were consolidated (Fig. 9 A). In numbers, the pore diameter decreases from 1.29 mm to 0.61 mm (Fig. 9 C) as well as the overall porosity from 64.73 % to 37.76 % (Fig. 9 D). This consolidation process could occur due to the gravitational force acting on printed strands and due to the additional weight of the higher layers. As a consequence, the scaffold structure appears bent due to strut sedimentation. The µ-CT evaluation of the examined hierarchical structure demonstrated how the physicochemical modification of gelatine improved the 3D printability of the ADA-GEL ink and enabled the tunability of the internal scaffold porosity gradient. This is an important characteristic of a biomimetic cartilage tissue engineering approach [2]. XZ and XY µ-CT images displayed decreasing pore diameters (from 1.45 mm to 0.23 mm) as well as decreasing overall XY plane porosities (from 81.66 % to 30.98 %) from

top to bottom (Fig. 9 C+D). This achieved tunability of pore sizes met tissue engineering demands. Pore sizes in the range of 20 µm - 500 µm are crucial in tissue engineering since they are suitable for cell ingrowth, bone regeneration as well as vascularization [52–54]. Furthermore, pore sizes and porosities were in the same order of magnitude compared to other 3D scaffold fabrication techniques for cartilage tissue engineering. For example, Tamaddon et al. [55] showed that freeze-dried type II collagen scaffolds with pore sizes ranging from 50 µm – 300 µm and an overall porosity of over 99 % featured a suitable environment for human bone marrow mesenchymal stem cells and their differentiation towards chondrocytes. However, chondrogenic differentiation was especially promoted by using chondroitin sulfate [55]. Lee et al. generated salt leached and solvent cast 3D scaffolds made of poly(L-lactide)-g-chondroitin for cartilage tissue engineering. An average pore size between 50 and 250 µm with an overall porosity of over 85 % was reported [56].

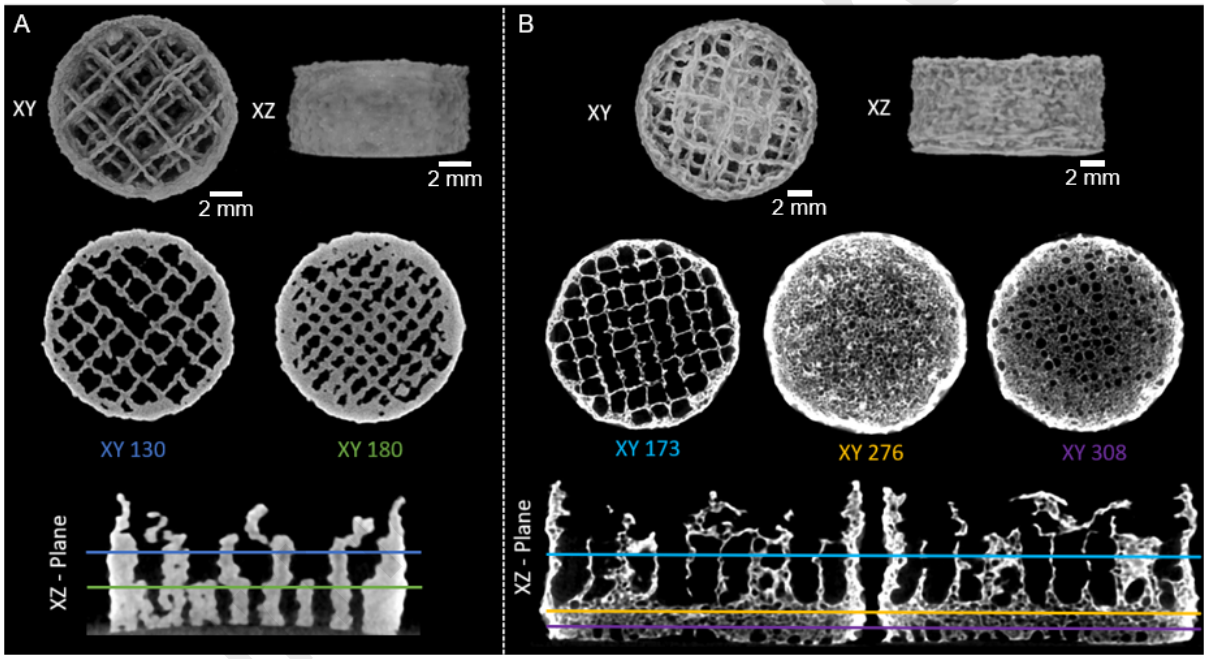

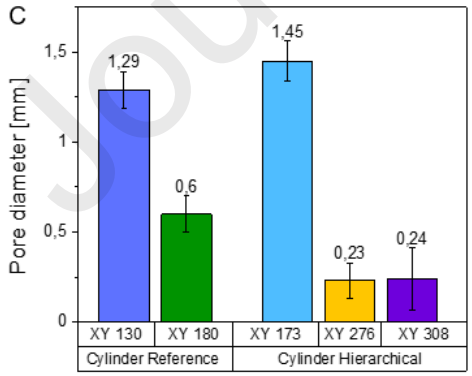

D

Cylinder XY Plane	Porosity [%]
Reference Cylinder XY 130	64.73
Reference Cylinder XY 180	37.76
Hierarchical Cylinder XY 173	81.66
Hierarchical Cylinder XY 276	30.98
Hierarchical Cylinder XY 308	33.25

Figure 9: µ-CT images of critical point dried ADA-GEL$_{80°C_3h}$ scaffolds. **A:** Reference Cylinder with consistent strut density. **B:** Hierarchical scaffold with varying strut densities (introduced in Fig. 8 A). **C:** Pore diameters. **D:** Porosities (absolute values) in XY planes.

4. Conclusions

In this study, hierarchical extrusion-based bioprinting of ADA-GEL was demonstrated for applications in cartilage tissue engineering. 3D-bioprinting was used to manufacture hierarchical scaffolds in a biomimetic approach to recapitulate the heterogeneous structure of the native cartilage tissue. Hydrogel precursor modification via thermal pre-treatment of gelatine enabled modifiable mechanical and rheological characteristics of the ADA-GEL material. Therefore, an advance in ADA-GEL hydrogel applications could be presented due to a significantly improved printability in comparison to previous studies [11]. Gelatine solutions were exposed to 37, 70, 80 and 95 °C for periods of 3 h and 6 h before ADA-GEL solution preparation and compared to prior investigated ADA-GEL compositions [57]. Substantiated by rheological characterization via time-, amplitude-, frequency-, recovery-, and temperature sweeps, ADA-GEL-$T_{80°C\_3h}$ was found to feature the most favourable printability characteristics, enabling hierarchical layer deposition with high shape stability. The new ADA-GEL formulation allowed the design of hierarchical scaffolds mimicking the intrinsic hierarchical structure of natural cartilage tissue. Scaffolds with heights of over 1 cm could be printed. µCT analysis confirmed the fabrication of open porous, hierarchically structured scaffolds. Therefore, in future experiments, these scaffolds combined with chondrocytes could offer a rapidly accelerated healing process for damaged or diseased cartilage tissue thanks to directed organized cell orientation and new tissue formation. Nanoindentation proved that the hydrogel stiffness could be tuned by varying the gelatine pre-treatment temperature as well as by varying the concentration and type of crosslinking divalent ions. In summary, the results have implications for advancing cartilage TE investigations. The scaffolds fabricated in this study could be used as complex-structured, 3D-printed hierarchical templates for in-vitro cell seeding in matrix-associated cartilage implant strategies in the future.

5. Acknowledgements

This research was funded by the Deutsche Forschungsgemeinschaft (DFG, German Research Foundation)-SFB 1270/1-299150580. The authors thank Dr Joachim Kaschta for his advice and the introduction to the rheometer and Eva Hufnagel for the support of the 3D volume analysis. Furthermore, the authors acknowledge the support from the project HY2Print (03XP0097C).

6. Author Contributions

T.D., R.D., A.R.B and T.K. conceptualized the work. A.R.B. had the project administration. A.R.B., T.D., and R.D. supervised the project. A.R.B. and R.D. provided the project resources. T.K. carried out the ADA-GEL characterisation (via FTIR, SDS-PAGE, Rheology, and Nanoindentation) as well as the printability assessment. T.K. wrote the G-code programme for resolution structures. Results were validated from S.H., T.D., and T.K. All results were analysed and visualised by T.K. S.G. carried out the µ-CT analysis. A.R.B., R.D., T.D., and T.K. discussed the results. T.K. wrote the original paper draft. T.D., S.H., S.G., R.D., and A.R.B. corrected and approved the paper draft.

7. References

[1] M. Rabenberg, Arthrose, Robert-Koch-Institut, Berlin, 2013.

[2] A.J. Sophia Fox, A. Bedi, S.A. Rodeo, The Basic Science of Articular Cartilage: Structure, Composition, and Function, Sport. Heal. A Multidiscip. Approach. (2009). https://doi.org/10.1177/1941738109350438.

[3] M. Hackenbroch, Arthrosen: Basiswissen zu Klinik, Diagnostik und Therapie, Georg Thieme Verlag, Stuttgart, 2002.

[4] E.B. Hunziker, Articular cartilage repair: basic science and clinical progress. A review of the current status and prospects, Osteoarthr. Cartil. (2002). https://doi.org/10.1053/joca.2002.0801.

[5] D. D'Lima, R. Bermejo, C. Colwell, A nonlinear viscoelastic finite element model evaluating the effects of autologous osteochondral grafting in the treatment of cartilage defects., in: 2002.

[6] J.L. Drury, D.J. Mooney, Hydrogels for tissue engineering: scaffold design variables and applications, Biomaterials. (2003). https://doi.org/10.1016/S0142-9612(03)00340-5.

[7] T.A. Mir, S. Iwanaga, T. Kurooka, H. Toda, S. Sakai, M. Nakamura, Biofabrication offers future hope for tackling various obstacles and challenges in tissue engineering and regenerative medicine: A Perspective, Int. J. Bioprinting. (2018). https://doi.org/10.18063/ijb.v5i1.153.

[8] L. Moroni, T. Boland, J.A. Burdick, C. De Maria, B. Derby, G. Forgacs, J. Groll, Q. Li, J. Malda, V.A. Mironov, C. Mota, M. Nakamura, W. Shu, S. Takeuchi, T.B.F. Woodfield, T. Xu, J.J. Yoo, G. Vozzi, Biofabrication: A Guide to Technology and Terminology, Trends Biotechnol. (2018). https://doi.org/10.1016/j.tibtech.2017.10.015.

[9] J.A. Rowley, G. Madlambayan, D.J. Mooney, Alginate hydrogels as synthetic extracellular matrix materials, Biomaterials. (1999). https://doi.org/10.1016/S0142-9612(98)00107-0.

[10] M.W. Tibbitt, K.S. Anseth, Hydrogels as extracellular matrix mimics for 3D cell culture, Biotechnol. Bioeng. (2009). https://doi.org/10.1002/bit.22361.

[11] T. Zehnder, A.R. Boccaccini, R. Detsch, Biofabrication of a co-culture system in an osteoid-like hydrogel matrix, Biofabrication. (2017). https://doi.org/10.1088/1758-5090/aa64ec.

[12] T. Distler, A.A. Solisito, D. Schneidereit, O. Friedrich, R. Detsch, A.R. Boccaccini, 3D printed oxidized alginate-gelatin bioink provides guidance for C2C12 muscle precursor cell orientation and differentiation via shear stress during bioprinting, Biofabrication. (2020). https://doi.org/10.1088/1758-5090/ab98e4.

[13] N. Soltan, L. Ning, F. Mohabatpour, P. Papagerakis, X. Chen, Printability and Cell Viability in Bioprinting Alginate Dialdehyde-Gelatin Scaffolds, ACS Biomater. Sci. Eng. (2019). https://doi.org/10.1021/acsbiomaterials.9b00167.

[14] Á.J. Leite, B. Sarker, T. Zehnder, R. Silva, J.F. Mano, A.R. Boccaccini, Bioplotting of a bioactive alginate dialdehyde-gelatin composite hydrogel containing bioactive glass nanoparticles, Biofabrication. (2016). https://doi.org/10.1088/1758-5090/8/3/035005.

[15] M.B. Łabowska, K. Cierluk, A.M. Jankowska, J. Kulbacka, J. Detyna, I. Michalak, A review on the adaption of alginate-gelatin hydrogels for 3D cultures and bioprinting, Materials (Basel). 14 (2021) 1–28. https://doi.org/10.3390/ma14040858.

[16] M. Park, D. Lee, J. Hyun, Nanocellulose-alginate hydrogel for cell encapsulation, Carbohydr. Polym. (2014). https://doi.org/10.1016/j.carbpol.2014.07.059.

[17] P. Siqueira, É. Siqueira, A.E. de Lima, G. Siqueira, A.D. Pinzón-Garcia, A.P. Lopes, M.E.C. Segura, A. Isaac, F.V. Pereira, V.R. Botaro, Three-dimensional stable alginate-nanocellulose gels for biomedical applications: Towards tunable mechanical properties and cell growing, Nanomaterials. 9 (2019) 1–22. https://doi.org/10.3390/nano9010078.

[18] A. Weizel, T. Distler, D. Schneidereit, O. Friedrich, L. Bräuer, F. Paulsen, R. Detsch, A.R. Boccaccini, S. Budday, H. Seitz, Complex mechanical behavior of human articular cartilage and hydrogels for cartilage repair, Acta Biomater. 118 (2020) 113–128. https://doi.org/10.1016/j.actbio.2020.10.025.

[19] T. Distler, K. McDonald, S. Heid, E. Karakaya, R. Detsch, A.R. Boccaccini, Ionically and Enzymatically Dual Cross-Linked Oxidized Alginate Gelatin Hydrogels with Tunable Stiffness and Degradation Behavior for Tissue Engineering, ACS Biomater. Sci. Eng. (2020). https://doi.org/https://doi.org/10.1021/acsbiomaterials.0c00677.

[20] B. Sarker, D.G. Papageorgiou, R. Silva, T. Zehnder, F. Gul-E-Noor, M. Bertmer, J. Kaschta, K. Chrissafis, R. Detsch, A.R. Boccaccini, Fabrication of alginate–gelatin crosslinked hydrogel microcapsules and evaluation of the microstructure and physico-chemical properties, J. Mater. Chem. B. (2014). https://doi.org/10.1039/c3tb21509a.

[21] T. Gao, G.J. Gillispie, J.S. Copus, A.K. PR, Y. Seol, A. Atala, J.J. Yoo, S.J. Lee, Optimization of gelatin–alginate composite bioink printability using rheological parameters: a systematic approach, Biofabrication. (2018). https://doi.org/10.1088/1758-5090/aacdc7.

[22] J.H. Muyonga, C.G.B. Cole, K.G. Duodu, Characterisation of acid soluble collagen from skins of young and adult Nile perch (Lates niloticus), Food Chem. (2004). https://doi.org/10.1016/j.foodchem.2003.06.006.

[23] T. Aewsiri, S. Benjakul, W. Visessanguan, Functional properties of gelatin from cuttlefish (Sepia pharaonis) skin as affected by bleaching using hydrogen peroxide, Food Chem. (2009). https://doi.org/https://doi.org/10.1016/j.foodchem.2008.12.012.

[24] H.D. Jeschkeit, H. Jakubke, Aminosäuren, Peptide, Proteine, 1982. https://doi.org/https://doi.org/10.1002/ciuz.19830170209.

[25] B. Sarmento, D. Ferreira, F. Veiga, A. Ribeiro, Characterization of insulin-loaded alginate nanoparticles produced by ionotropic pre-gelation through DSC and FTIR studies, Carbohydr. Polym. (2006). https://doi.org/10.1016/j.carbpol.2006.02.008.

[26] R.M. Issa, A.M. Khedr, H. Rizk, 1H NMR , IR and UV / VIS Spectroscopic Studies of Some Schiff Bases Derived From 2-Aminobenzothiazole and 2-Amino-3-hydroxypyridine, J. Chinese Chem. Soc. (2008). https://doi.org/10.1002/jccs.200800131.

[27] S. Hoque, S. Benjakul, T. Prodpran, Effect of heat treatment of film-forming solution on the properties of film from cuttlefish (Sepia pharaonis) skin gelatin, J. Food Eng. (2010). https://doi.org/10.1002/jccs.200800131.

[28] S. Gorgieva, V. Kokol, Collagen-vs. Gelatin-Based Biomaterials and Their Biocompatibility : Review and Perspectives, Biomater. Appl. Nanomedicine. (2011). https://doi.org/10.5772/24118.

[29] B. Sarker, Advanced Hydrogels Concepts Based on Combinations of Alginate , Gelatin and Bioactive Glasses for Tissue Engineering, Dr. Diss. Friedrich-Alexander-Universität Erlangen-Nürnb. (2015).

[30] Sigma-Aldrich, Product information of gelatin, (2016).

[31] E. van den Bosch, C. Gielens, Gelatin degradation at elevated temperature, Int. J. Biol. Macromol. (2003). https://doi.org/10.1016/S0141-8130(03)00046-1.

[32] M. Djabourov, J. Leblond, P. Papon, Gelation of aqueous gelatin solutions, J. Phys. (1988). https://doi.org/10.1051/jphys:01988004902031900.

[33] L. Ouyang, R. Yao, Y. Zhao, W. Sun, Effect of bioink properties on printability and cell viability for 3D bioplotting of embryonic stem cells, Biofabrication. (2016). https://doi.org/10.1088/1758-5090/8/3/035020.

[34] A. Tirella, A. Orsini, G. Vozzi, A. Ahluwalia, A phase diagram for microfabrication of geometrically controlled hydrogel scaffolds, Biofabrication. (2009). https://doi.org/10.1088/1758-5082/1/4/045002.

[35] N. Paxton, W. Smolan, T. Böck, F. Melchels, J. Groll, T. Jungst, Proposal to assess printability of bioinks for extrusion-based bioprinting and evaluation of rheological properties governing bioprintability, Biofabrication. (2017). https://doi.org/https://doi.org/10.1088/1758-5090/aa8dd8.

[36] W. Liu, M.A. Heinrich, Y. Zhou, A. Akpek, N. Hu, X. Liu, X. Guan, Z. Zhong, X. Jin, A. Khademhosseini, Y.S. Zhang, Extrusion Bioprinting of Shear-Thinning Gelatin Methacryloyl Bioinks, Adv. Healthc. Mater. (2017). https://doi.org/10.1002/adhm.201601451.

[37] MalvernInstruments, A Basic Introduction to Rheology, (2016). https://cdn.technologynetworks.com/TN/Resources/PDF/WP160620BasicIntroRheology.pdf.

[38] R. Schrieber, H. Gareis, Gelatine Handbook - Theory and Industrial Practice, WILEY-VCH, 2007. https://doi.org/10.1002/9783527610969.

[39] T. Distler, L. Kretzschmar, D. Schneidereit, S. Girardo, R. Goswami, O. Friedrich, R. Detsch, J. Guck, A.R. Boccaccini, S. Budday, Mechanical properties of cell- and microgel bead-laden oxidized alginate-gelatin hydrogels, Biomater. Sci. (2021). https://doi.org/10.1039/D0BM02117B.

[40] T. Billiet, E. Gevaert, T. De Schryver, M. Cornelissen, P. Dubruel, The 3D printing of gelatin methacrylamide cell-laden tissue-engineered constructs with high cell viability, Biomaterials. 35 (2014) 49–62. https://doi.org/10.1016/j.biomaterials.2013.09.078.

[41] E. Boanini, K. Rubini, S. Panzavolta, A. Bigi, Chemico-physical characterization of gelatin films modified with oxidized alginate, Acta Biomater. (2010). https://doi.org/10.1016/j.actbio.2009.06.015.

[42] C. Remuñán-López, R. Bodmeier, Mechanical, water uptake and permeability properties of crosslinked chitosan glutamate and alginate films, J. Control. Release. (1997). https://doi.org/10.1016/S0168-3659(96)01525-8.

[43] D. Poncelet, V. Babak, C. Dulieu, A. Picot, A physico-chemical approach to production of alginate beads by emulsification-internal ionotropic gelation, Colloids Surfaces A Physicochem. Eng. Asp. (1999). https://doi.org/10.1016/S0927-7757(98)00709-2.

[44] A. Skardal, D. Mack, A. Atala, S. Soker, Substrate elasticity controls cell proliferation, surface marker expression and motile phenotype in amniotic fluid-derived stem cells, J. Mech. Behav. Biomed. Mater. (2013). https://doi.org/10.1016/j.jmbbm.2012.10.001.

[45] M. Akhmanova, E. Osidak, S. Domogatsky, S. Rodin, A. Domogatskaya, Physical, Spatial, and Molecular Aspects of Extracellular Matrix of In Vivo Niches and Artificial Scaffolds Relevant to Stem Cells Research, Stem Cells Int. (2015). https://doi.org/10.1155/2015/167025.

[46] F. Guilak, L.G. Alexopoulos, M.A. Haider, H.P. Ting-Beall, L.A. Setton, Zonal Uniformity in Mechanical Properties of the Chondrocyte Pericellular Matrix: Micropipette Aspiration of Canine Chondrons Isolated by Cartilage Homogenization, Ann. Biomed. Eng. (2005). https://doi.org/10.1007/s10439-005-4479-7.

[47] K.A. Homan, D.B. Kolesky, M.A. Skylar-Scott, J. Herrmann, H. Obuobi, A. Moisan, J.A. Lewis, Bioprinting of 3D Convoluted Renal Proximal Tubules on Perfusable Chips, Sci. Rep. (2016). https://doi.org/10.1038/srep34845.

[48] K.Y. Lee, D.J. Mooney, Alginate: Properties and biomedical applications, Prog. Polym. Sci. (2012). https://doi.org/10.1016/j.progpolymsci.2011.06.003.

[49] C.C. Chang, E.D. Boland, S.K. Williams, J.B. Hoying, Direct-write bioprinting three-dimensional biohybrid systems for future regenerative therapies, J. Biomed. Mater. Res. Part B Appl. Biomater. (2011). https://doi.org/10.1002/jbm.b.31831.

[50] R. Chang, J. Nam, W. Sun, Effects of Dispensing Pressure and Nozzle Diameter on Cell Survival from Solid Freeform Fabrication–Based Direct Cell Writing, Tissue Eng. Part A. (2008). https://doi.org/10.1089/ten.a.2007.0004.

[51] D.B. Kolesky, K.A. Homan, M.A. Skylar-Scott, J.A. Lewis, Three-dimensional bioprinting of thick vascularized tissues, Proc. Natl. Acad. Sci. (2016). https://doi.org/10.1073/pnas.1521342113.

[52] N. Annabi, J.W. Nichol, X. Zhong, C. Ji, S. Koshy, A. Khademhosseini, F. Dehghani, Controlling the Porosity and Microarchitecture of Hydrogels for Tissue Engineering, Tissue Eng. Part B Rev. (2010). https://doi.org/10.1089/ten.teb.2009.0639.

[53] K. Whang, K.E. Healy, D.R. Elenz, E.K. Nam, D.C. Tsai, C.H. Thomas, G.W. Nuber, F.H. Glorieux, R. Travers, S.M. Sprague, Engineering Bone Regeneration with Bioabsorbable Scaffolds with Novel Microarchitecture, Tissue Eng. (1999). https://doi.org/10.1089/ten.1999.5.35.

[54] M.C. Wake, C.W. Patrick, A.G. Mikos, Pore Morphology Effects on the Fibrovascular Tissue Growth in Porous Polymer Substrates, Cell Transplant. (1994). https://doi.org/10.1177/096368979400300411.

[55] M. Tamaddon, M. Burrows, S.A. Ferreira, F. Dazzi, J.F. Apperley, A. Bradshaw, D.D. Brand, J. Czernuszka, E. Gentleman, Monomeric, porous type II collagen scaffolds promote chondrogenic differentiation of human bone marrow mesenchymal stem cells in vitro, Sci. Rep. (2017). https://doi.org/10.1038/srep43519.

[56] C.-T. Lee, C.-P. Huang, Y.-D. Lee, Biomimetic Porous Scaffolds Made from Poly(l -lactide)-g-chondroitin Sulfate Blend with Poly(l-lactide) for Cartilage Tissue Engineering, Biomacromolecules. (2006). https://doi.org/10.1021/bm060451x.

[57] B. Sarker, T. Zehnder, S.N. Rath, R.E. Horch, U. Kneser, R. Detsch, A.R. Boccaccini, Oxidized Alginate-Gelatin Hydrogel: A Favorable Matrix for Growth and Osteogenic Differentiation of Adipose-Derived Stem Cells in 3D, ACS Biomater. Sci. Eng. (2017). https://doi.org/10.1021/acsbiomaterials.7b00188.

Graphical abstract

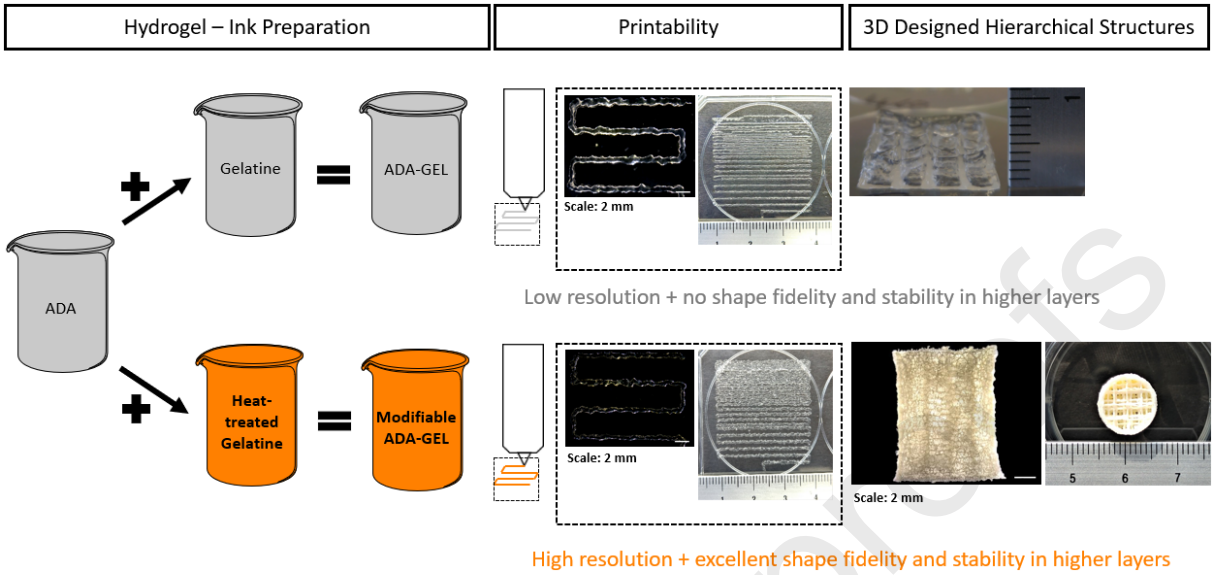

Highlights:

- Bioprinting of alginate dialdehyde-gelatine demonstrated for cartilage tissue engineering
- Thermal pre-treatment of gelatine affects hydrogel mechanical and rheological characteristics
- Thermal pre-treatment of gelatine enables 3D printing of hierarchical complex structures

Credit Author Statement

T.D., R.D., A.R.B and T.K. conceptualized the work. A.R.B. had the project administration. A.R.B., T.D., and R.D. supervised the project. A.R.B. and R.D. provided the project resources. T.K. carried out the ADA-GEL characterisation (via FTIR, SDS-PAGE, Rheology, and Nanoindentation) as well as the printability assessment. T.K. wrote the G-code programme for resolution structures. Results were validated from S.H., T.D., and T.K. All results were analysed and visualised by T.K. S.G. carried out the μ-CT analysis. A.R.B., R.D., T.D., and T.K. discussed the results. T.K. wrote the original paper draft. T.D., S.H., S.G., R.D., and A.R.B. corrected and approved the paper draft.

Physico-chemical Modification of Gelatine for the Improvement of 3D Printability of Oxidized Alginate-gelatine Hydrogels Towards Cartilage Tissue Engineering

T. Kreller[1*], T. Distler[1*], S. Heid[1], S. Gerth[2], R. Detsch[1], A. R. Boccaccini[1§]

[1]Institute of Biomaterials, Department of Materials Science and Engineering, Friedrich Alexander-University Erlangen-Nürnberg, 91058 Erlangen, Germany
[2]Fraunhofer Institute for Integrated Circuits IIS

[*]equal contribution
[§]corresponding author: aldo.boccaccini@fau.de

The authors declare no conflict of interest.